Journal of Non-Crystalline Solids 492 (2018) 1–10

Contents lists available at ScienceDirect

Journal of Non-Crystalline Solids

journal homepage: www.elsevier.com/locate/jnoncrysol

Marl-based geopolymers incorporated with limestone: A feasibility study

Nailia R. Rakhimova[a,*], Ravil Z. Rakhimov[b], Vladimir P. Morozov[c], Albert R. Gaifullin[b], Ludmila I. Potapova[d], Alfiya M. Gubaidullina[e], Yury N. Osin[f]

[a] Faculty of Civil Engineering, Ton Duc Thang University, Ho Chi Minh City, Vietnam
[b] Department of Building Materials, Kazan State University of Architecture and Engineering, Kazan, Russian Federation
[c] Department of mineralogy and lithology, Kazan Federal University, Kazan, Russian Federation
[d] Department of physics, electrical and automatic engineering, Kazan State University of Architecture and Engineering, Kazan, Russian Federation
[e] Central Research Institute for Geology of Industrial Minerals, Kazan, Russian Federation
[f] Interdisciplinary Center for Analytical Microscopy Kazan Federal University, Kazan, Russian Federation

ARTICLE INFO

Keywords:
Kaolinite
Marl
Geopolymer
Microstructure
Mechanical properties

ABSTRACT

The expanding raw materials base is one of the drivers for the further development of inorganic binders, including alkali-activated cements. This research focuses on studying marl with a high calcite/aluminosilicates ratio as a geopolymer precursor, and limestone as a mineral addition to this geopolymer. The calcination of marl at 800 °C resulting in the formation of reactive Si, Al, and Ca due to the dehydroxylation of clay minerals and decarbonation of calcite makes marl suitable for use as a geopolymer precursor. Calcined marl activated with sodium silicate and cured at ambient temperature had a 28-day compressive strength of 34 MPa. When incorporated with 50% limestone, the compressive strength became 39.2 MPa. XRD, TG/DSC, FTIR, optical and SEM have been used to investigate the reaction products, as well as the microstructure of the geopolymer hardened pastes.

1. Introduction

Geopolymerization, as a non-fire or low-temperature production method of binders based on various natural and technogenic aluminosilicate materials that are not inferior to the properties of Portland cement, increasingly appeals both in theory and practice [1,2]. Progress in this area is also driven by the constant expansion of the raw material base and the possibilities of using a wide range of both natural and waste aluminosilicate materials [3,4]. The use of different aluminosilicate precursors and ways to improve the performance of the geopolymers based on them through the introduction of chemical additives and mineral additions are also being researched and developed [5–8].

The increasing importance of thermally activated clays as supplementary cementitious materials for Portland cement [9–13] and as precursors for alkali-activated materials [1,2] should be noted. The most valuable clay for both Portland cement-based and alkali-activated cements is metakaolin, which is produced by heating kaolin clays. However, the scarcity of their reserves and the associated high costs have led to research in different countries involving feasibility studies on the use of the more common low-grade kaolin clays and other clays consisting of different minerals [14–18] including calcined marl [19]. Many studies stated the possibility of transforming a wide range of clays or natural and synthetic aluminosilicates like the smectite and the smectite/illite-types of clays [20,21], 16 aluminosilicate minerals with different structures and compositions (albite, illite, sillimanite, andalusite, and others) [22,23], halloysite [24], feldspars [17], etc. into alkali-activated cements. The mechanical performance of the alkaline cements obtained with common clay and feldspar is lower as a rule than that of the cements synthesized from fly ash or metakaolin (MK) [1].

The combination of calcined clays with calcium aluminosilicates (high-calcium fly ash, or slag) [25–30] and fillers is an effective way to reduce the dependence on aluminosilicate clay sources and manage the macro-, micro-, and nanostructures, as well as the technological and physical and technical characteristics of such blended activated systems.

One of the most used mineral additions, both for the blended Portland cements and non-clinker cements, is limestone [31–44]. In the case of alkali-activated cements, a combination of aluminosilicate precursors with physically or chemically active supplementary materials or with materials that are both physically and chemically active is effective because alkali activation allows not only the production of alkali-activated cements of superior technical efficiency in matrices, but also allows for an effective interaction between the alkali-activated cement paste and the fillers, as well as compatibility with mineral

* Corresponding author at: 19 Nguyen Huu Tho, Tan Phong Ward, District 7, Ho Chi Minh City 700000, Vietnam.
E-mail address: nailia.rakhimova@tdt.edu.vn (N.R. Rakhimova).

https://doi.org/10.1016/j.jnoncrysol.2018.04.015
Received 14 February 2018; Received in revised form 5 April 2018; Accepted 7 April 2018

blending materials of various compositions and structures [6].

As to MK and limestone LS, several studies have been conducted on the beneficial results of their combination.

According to Yip's study [44], the introduction of 20 wt%. of calcite into MK activated by a sodium silicate solution (SiO_2/Na_2O ratio of 1.2:2) is found to improve the mechanical strength of the geopolymer. The authors explained that the results obtained were due to the contributions of the calcium and magnesium ions to the increased adhesion between the particles and the polymeric gel. However, the contribution of these ions in the polymerization process wasn't found to be significant.

In a study of the MK-LS-NaOH system, Cwirzen [36] stated that the presence of LS enhances the release of Al and Si ions from MK. The amount of leached Ca was generally low in all cases, independent of the LS/MK ratio. The concentration of dissolved calcium decreased with time probably due to solution saturation effects and a reduction in the solubility of Ca as the dissolved Si concentration increased. From these data, it was concluded that a small amount of Ca released from LS at an early stage hindered the initial release of Al and Si from MK. However, the authors believe that the actual mechanism is more complex, and involves a complexation and reprecipitation/gel formation process rather than direct hindrance. The newly formed precipitates may be forming on the unreacted particle surfaces, thus creating a degree of hindrance, but this is likely to be a secondary effect. Later, when the dissolved Ca concentration is lower, the release of Al and Si increases. The main alkali-activation product in the investigated pastes is a geopolymer gel with inclusions of unreacted MK, LS particles, zeolite A, and calcium aluminate monosulphates, with different zeolites such as faujasite-like and hydrosodalite phases also identified at higher reaction temperatures. The replacement of MK by 50% LS increased the strength of the hardened paste from 4 to 5 MPa at a curing temperature of 20 °C and from 5 to 7 MPa at a curing temperature of 80 °C.

Aboulayt [45] found that a highly basic environment does not promote the dissolution of calcite, the latter acts as an inert filler in replacing MK. Low amounts of Ca^{2+} ions in the initial mixture do not cause variations in the activation energy.

Qian and Song [46] reported that the addition of up to 10% LS to MK activated by potassium hydroxide improved the mechanical properties and the workability of the fresh geopolymer. The authors attributed this to the formation of a more compact structure and a better particle size distribution and refer to it as the “filler effect”.

This research aims to study the properties, the reaction products and the microstructure of a sodium silicate activated geopolymer based on calcined marl (CM) with a high calcite/clay minerals ratio that also incorporates LS.

2. Experimental details

2.1. Materials

The marl and LS used in this study were obtained from deposits from the Republic of Tatarstan (Russian Federation). The marl had the following mineral composition (wt%): kaolinite – 3.45%, montmorillonite – 6.45%, clinochlore – 1.12%, calcite – 57.08%, quartz – 12.58%, orthoclase – 8.42%, muscovite – 6.37%, gypsum – 4.57%, amorphous phase – 34%. The LS had the following mineral composition (wt%): calcite – 90%, quartz – 9%, albite – 1%. The chemical compositions of the starting materials are shown in Table 1, and the details of the size distributions are given in Fig. 1. The specific surface area of marl was 5000 cm^2/g, and that of limestone was 3700 cm^2/g (Blaine). SEM images of the marl are shown in Fig. 2.

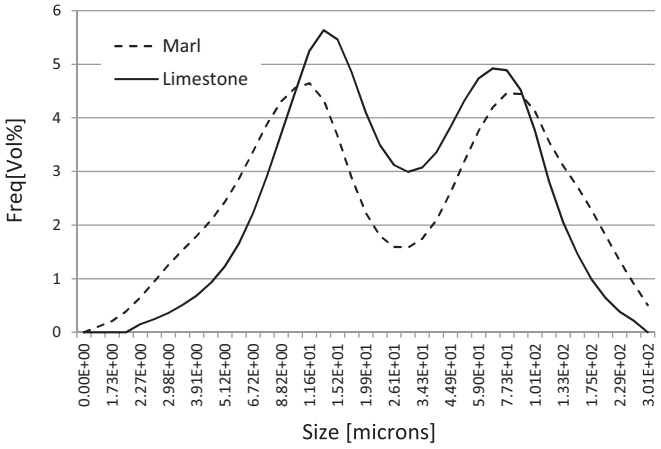

Fig. 1. Particle size distribution of the raw materials measured by laser granulometry.

The alkaline activator commercial hydrous sodium metasilicate $Na_2SiO_3{\cdot}5H_2O$ (NSH_5) was obtained from Meterra (Russian Federation), the molar ratio of silica to sodium ($M_s = SiO_2/Na_2O$) is 1.

2.2. Methods

The marl was calcined at 600, 700, and 800 °C using heating rates of 1.7, 2.5 and 3.3 °C/min, respectively. A dwell time of 3 h was used.

The starting materials were milled in a MPL-1 laboratory planetary mill.

The NSH_5 solution was obtained by dissolving NSH_5 in deionized water and cooling down to room temperature during 24 h prior to use.

The reference sample was prepared by 2 min mixing of CM and NSH_5 solution. The mixed compositions of CM and LS were dry-premixed for 2 min, the NSH_5 solution was then added and the pastes were mixed for a further 2 min. Mixture proportions of the pastes are presented in Table 2. A liquid/solid ratio of 0.4–45 provided a workable and appropriate flowability of the fresh pastes and decreased with the increase of the LS content. The geopolymer paste samples were prepared in cubic moulds (2 × 2 × 2 cm) for compressive strength tests and then demoulded after two days. The cubes were stored in sealed plastic bags in a chamber at room temperature and 98% relative humidity for 28 days. Compression tests were performed by applying a load between the two surfaces that were vertical during casting. Each strength determination quoted is based on an average of six measurements from the same cast.

Calorimetry experiments were carried out using a “Thermochron” measuring device. The pastes were mixed externally, placed in sealed glass ampoules, and loaded into the calorimeter. The time elapsed between the addition of the activating solution to the powder and the loading of the paste into the calorimeter was approximately 3–4 min. The tests were run for 24 h.

Table 1
Chemical composition of starting materials.

Starting material	Component (mass % as oxide)												
	SiO_2	CaO	Al_2O_3	MgO	MnO	Fe_2O_3	TiO_2	Na_2O	K_2O	P_2O_5	SO_3	CO_2	LOI
Raw marl	40.30	40.00	9.04	0.82	–	4.40	0.41	0.51	0.93	0.40	0.05	–	3.55
Calcined marl	40.56	40.26	9.3	1.08	–	4.66	0.67	0.77	1.19	0.66	0.31	–	0.60

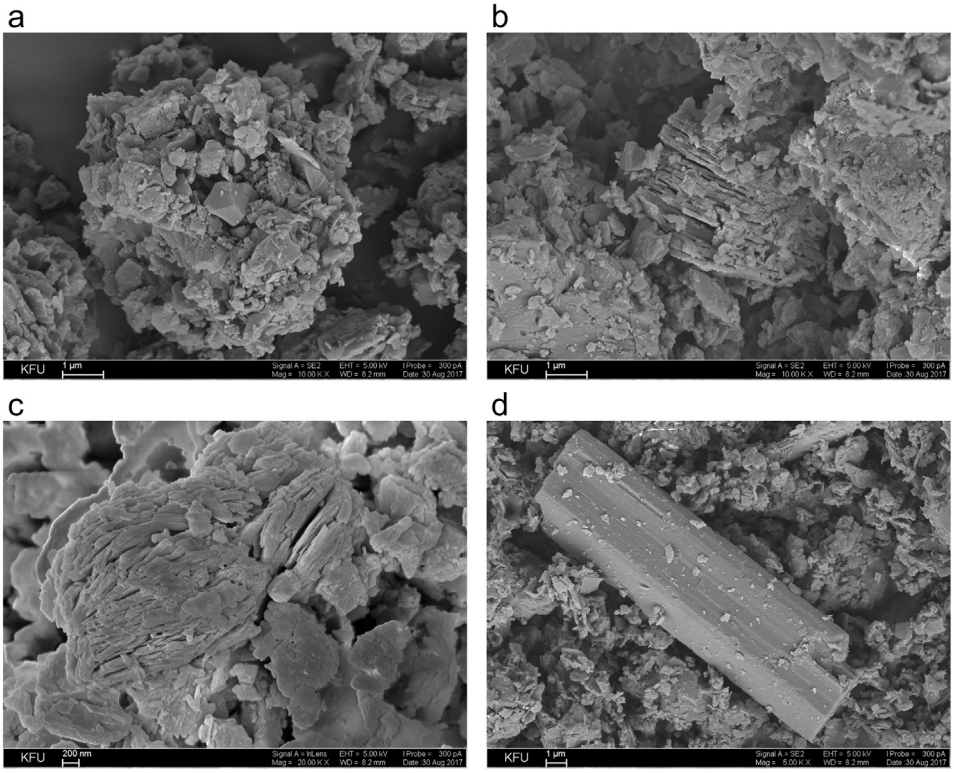

Fig. 2. SEM images of the marl: a) particle of the marl, b),c) kaolinite, d) mica.

Table 2
Mixture proportions of pastes.

Sample	Unit weight (g)			
	CM	LS	NSH_5	Deionized water
CM 100	1000	–	501	450
CM75/LS25	750	250	501	430
CM50/LS50	500	500	501	400

X-ray diffraction (XRD) and thermal analyses (TG/DSC) were performed on crushed samples that had been aged for 28 days. The XRD data were collected using a D2 Phaser X-ray diffractometer in a Bragg-Brentano θ–2θ configuration with a CuKα radiation, operating at 40 kV and 30 mA. The data analysis was performed using the DIFFRAC plus Evaluation Package EVA Search/Match and the PDF-2 ICDD database. The content of amorphous phase in RM and CM was estimated by analyzing the X-ray diffractograms in the software product Diffrac.eva V3.2. An STA 443 F3 Jupiter simultaneous thermal analysis apparatus was used for TG/DSC. The samples were heated from 30 °C to 1000 °C at a heating rate of 10 °C/min. The data was analysed using Netzsch Proteus Thermal Analysis.

FTIR spectra were recorded using a Spectrum 65 (Perkin-Elmer) ranging from 4000 to 650 cm^{-1}.

After 28 days of curing, the fragments of the selected samples for optical and scanning electron microscopy (SEM; Merlin of CARL ZEISS) observations were prepared by embedding them in an epoxy resin, followed by polishing, and carbon coating.

3. Results and discussion

3.1. Materials characterization

To determine the optimal calcination temperature and alkali concentration for the marl-based geopolymer, we performed preliminary studies on the influence of calcination temperature at 600, 700 and 800 °C for the alkali activator concentrations of 5, 10, and 15% respectively (by Na_2O by dry weight of starting materials) on the strength of the CM-based geopolymer. It was found that a compressive strength no lower than 30 MPa may be obtained when the calcination temperature of the marl was 800 °C and the concentration of NSH_5 was 15% (by Na_2O). These starting parameters have been accepted in this study.

Figs. 3 and 4 show the X-rays and thermal analyses of the raw marl (RM) and CM. Mineral compositions of RM and CM are presented in Table 3. X-ray analysis of RM shows that it consists of kaolinite, montmorillonite, clinochlore, calcite, quartz, orthoclase, muscovite, gypsum. The calcination of RM results in decomposition and the disappearance of the peaks assigned to gypsum, and clay minerals (montmorillonite, kaolinite, and clinochlore), and the appearance of anhydrite and larnite. Thermal treatment of montmorillonite, kaolinite, and clinochlore leads to their decomposition to an amorphous phase. The increase of the amorphous phase in CM compared to RM is also evident from Fig. 3 and it is approximately from 61 to 34%, respectively.

The thermal analysis for RM, Fig. 4, shows endothermic peaks at 45 °C - loss of adsorbed water, 120 °C - loss of crystallization water by montmorillonite and gypsum, 510 °C – dehydroxylation of kaolinite, 760 °C – dehydroxylation of kaolinite and decarbonation of calcite, exothermic peaks at 780 °C, 870 °C, 920 °C and 970 °C – calcium silicate (larnite) formation. The highest mass loss is detected at a temperatures range 630–780 °C – 19.31%, and total mass loss is 26.99%. The thermal analysis for CM, Fig. 4, show endothermic peaks at 200 °C, 370 °C and 450 °C – further dehydroxylation of residual clay minerals, 620 °C - decarbonation of calcite, exothermic peaks at 890 °C, 960 °C - larnite formation. Total mass loss of CM is 2.29%.

Fig. 5 shows the infrared spectroscopic results for RM, CM, and LS. The bands at 1415, 1417 cm^{-1}, 712, 871 cm^{-1}, 2530, 1800 cm^{-1}, which are observed in the spectra of all materials, are attributed to calcium carbonates [47–51]. The 3620 and 912 bands are related to OH– and Al–OH, respectively [52,53]. The appearance of the 1003 cm^{-1} band on the CM spectra indicates a change in the Si

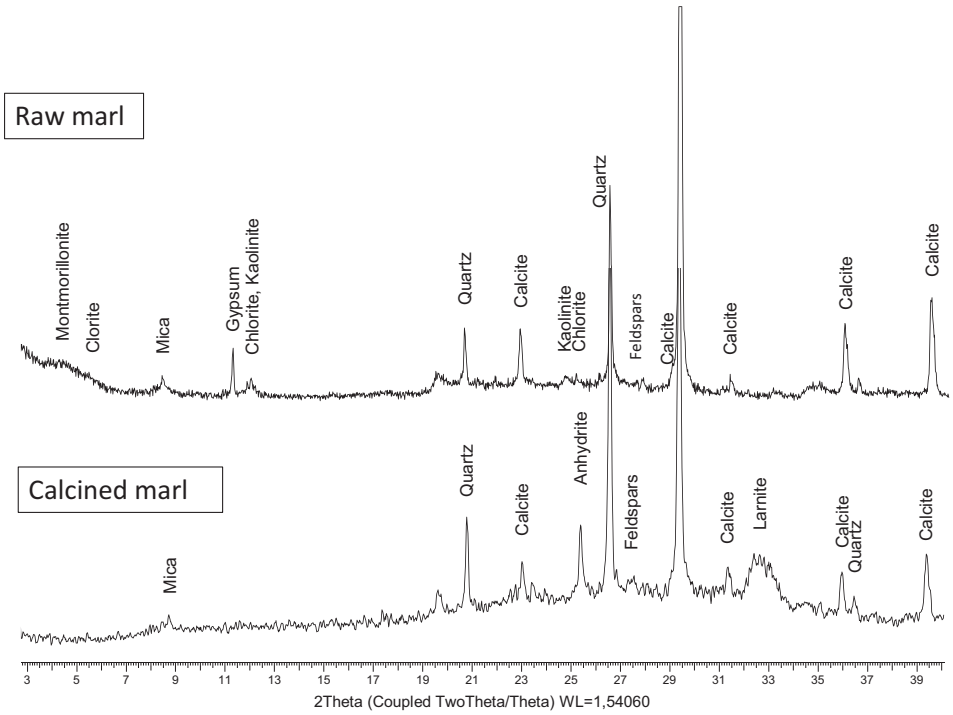

Fig. 3. X-ray diffractograms of RM and CM.

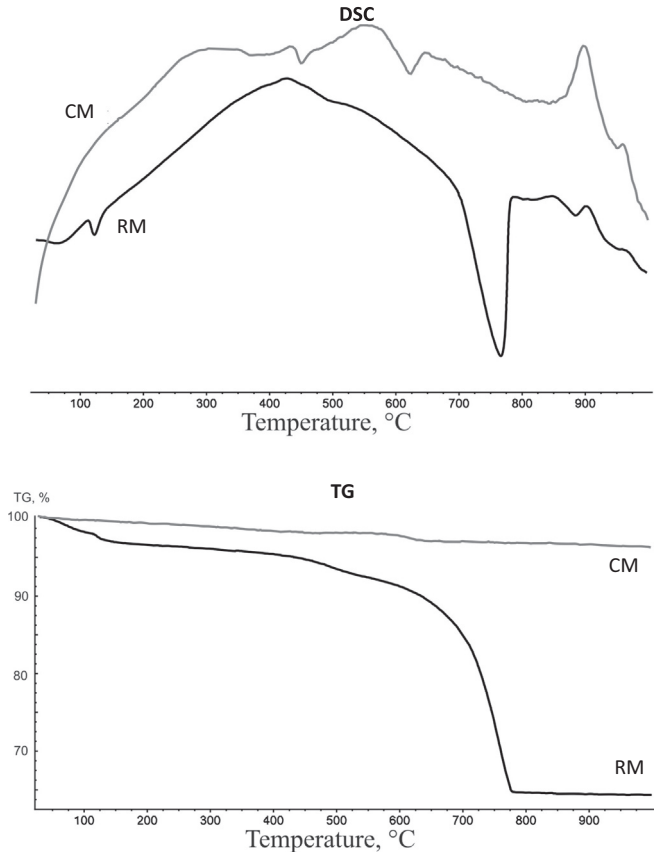

Fig. 4. Thermal analyses (TG/DSC) of RM and CM.

environment after calcination and is due to metakaolinite [53,54].

3.2. Mechanical properties

The influence of the quantity of LS on the 28-day compressive strength of the hardened geopolymer paste is shown in Fig. 6. As can be seen from the above data, the introduction of up to 50% LS leads to an improvement in compressive strength from 34 to 39.2 MPa. Further replacement of CM by LS notably deteriorates the strength of the hardened paste.

These data are in agreement with Cwirzen's study [36], wherein MK was replaced by 30 and 50 wt% LS; it was found that this slightly increased the 28 day compressive strength values in the case of 50 wt% replacement when a 5 M NaOH activator was used.

3.3. Heat release

Fig. 7 depicts the progress of the reactions of a fresh geopolymer paste based on CM and that incorporated with 25 and 50% LS. As can be seen, the pastes are characterized by two peaks. Thus, our results in terms of the two peaks are in agreement with the study of Rahier [54]. The first peak is attributed to the dissolution of the aluminosilicate precursor and the second one to the polymerization process. The presented results show that incorporating LS into the CM-based geopolymer causes delays in the reactions in the CM-NSH_5 system proportional to the LS content. The introduction of 25% LS into the CM-based geopolymer reduces the temperature of the first peak from 26 to 25.5 °C, and shifts its appearance from 20 to 30 min (reference sample CM100) to 30–70 min; it also reduces the temperature corresponding to the second peak from 28 to 26 °C and shifts its appearance from 310 min (reference sample CM100) to 400–660 min. For the CM50/LS50- NSH_5 system there was only one registered peak at a temperature of 25.5 °C at 50–120 min.

Table 3
Mineral compositions of RM and CM.

Raw marl	Calcined marl	PDF of minerals
Kaolinite $Al_2Si_2O_5(OH)_4$	–	(PDF 00-058-2028)
Montmorillonite $Na_{0.3}(AlMg)_2Si_4O_{10}(OH)_26H_2O$	–	(PDF 00-012-0219)
Clinochlore $(Mg_{2.96}Fe_{1.55}Fe_{0.136}Al_{1.275})$ $(Si_{2.622}Al_{1.37}6O_{10})(OH)_8$	–	(PDF 01-079-1270)
Calcite $CaCO_3$	Calcite $CaCO_3$	(PDF 00-005-0586)
Quartz SiO_2	Quartz SiO_2	(PDF 01-079-1910)
Orthoclase $KAlSi_3O_8$	Orthoclase $KAlSi_3O_8$	(PDF 00-022-1212)
Muscovite $KAl_2Si_3AlO_{10}(OH)_2$	Muscovite $KAl_2Si_3AlO_{10}(OH)_2$	(PDF 00-007-0025)
–	Anhydrite $CaSO_4$	(PDF 00-037-1496)
–	Larnite Ca_2SiO_4	(PDF 00-009-0351)

3.4. The influence of LS on the composition of hydration products and microstructure of hardened pastes

3.4.1. X-ray diffraction

The XRD patterns of the samples of hardened pastes of 100% CM (CM100), 50% LS content (CM50/LS50), and 75% LS content (CM25/LS75) are presented in Fig. 8. In the CM25/LS75 and CM50/LS50 samples, calcite and quartz are identified. In the sample CM100, larnite and orthoclase are also detected.

3.4.2. Thermal analysis

Figs. 9 and 10 show the results of TG/DSC. An analysis of these figures shows endothermic peaks on the thermal analysis curves. The first endothermic peak is in the range 50–150 °C, and is attributed to the presence of the N-A-S-H and/or C-A-S-H gels and the loss of evaporable water from the binder gels [36]. The CM100, CM50/LS50, and CM25/LS75 samples lose about 5.96, 9.19, and 1.89% of their mass, respectively in this temperature range. The second peak is in the 630–730 °C range for the CM100 sample, 640–750 °C range for the CM50/LS50 sample, and 650–780 °C range for the CM25/LS75 sample, while the associated mass losses are 10.38, 12.04, and 22.16%, respectively. This second endothermic peak is related to the decarbonation of calcite, and the mass loss increases with the increase of LS content in CM-based geopolymers.

3.4.3. FTIR analysis

Fig. 11 shows the infrared spectroscopic results. As can be seen from Fig. 11, the band related to metakaolinite (1003 cm^{-1}) disappeared, which indicates that metakaolinite was involved in the geopolymerization reactions. Along with the bands which are distinctive to calcite

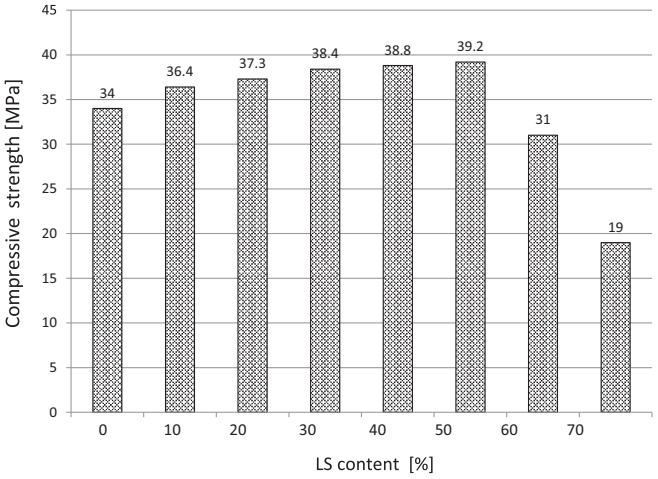

Fig. 6. Effect of LS content on 28-day compressive strength of the hardened pastes.

for the CM100, CM50/LS50, and CM25/LS75 samples the following structural characteristics are detected:

- the 3391, 3383, and 3389 cm^{-1} bands, representing the stretching and the deformation vibrations of OH− and H−O−H, and can be related to the atmospheric and bound water in the geopolymer gel [48,55],
- the 1648 cm^{-1} band, which is related to the bending vibrations (H−O−H) and is distinctive for polymeric structures, including

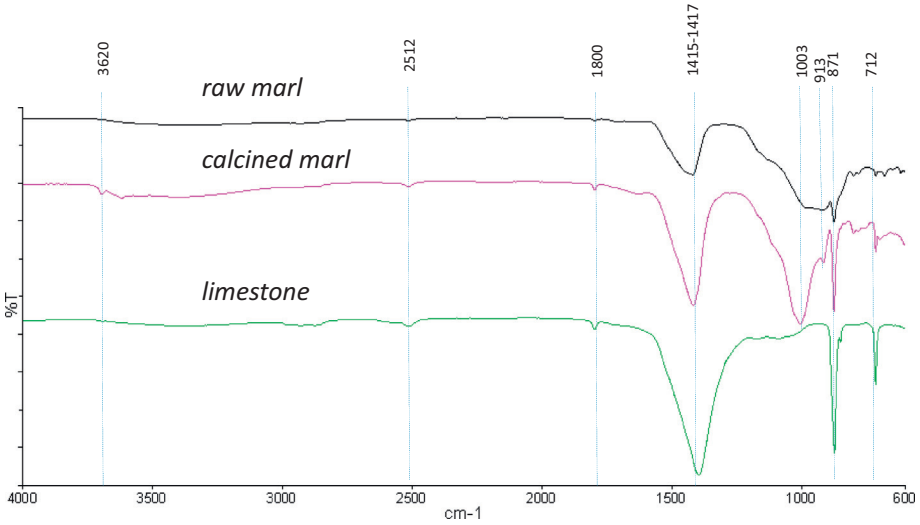

Fig. 5. FTIR spectra of RM, CM, and LS.

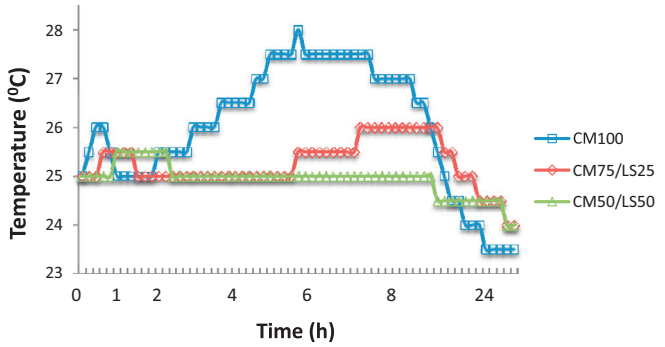

Fig. 7. Progress of the reactions of the fresh geopolymer paste based on metakaolin and that incorporated with 25 and 50% of LS.

aluminosilicate networks [56],
- the 948, 982, and 950 cm^{-1} bands, which represent the Si—O—T (T = Si or Al) asymmetric stretching vibrations and can be attributed to both N-A-S-H and C-A-S-H [57–59].

3.4.4. Analysis of the hardened pastes – optical microscopy, SEM

Figs. 12 and 13 show the results of optical microscopy, and Fig. 14 reveals the results of SEM. As can be seen, there is a good interaction in the transitional zone between the CM-based matrix and the LS particles. This observation is in agreement with the previous studies which found satisfactory surface binding between the LS powder and alkali-activated inorganic matrices [36,60].

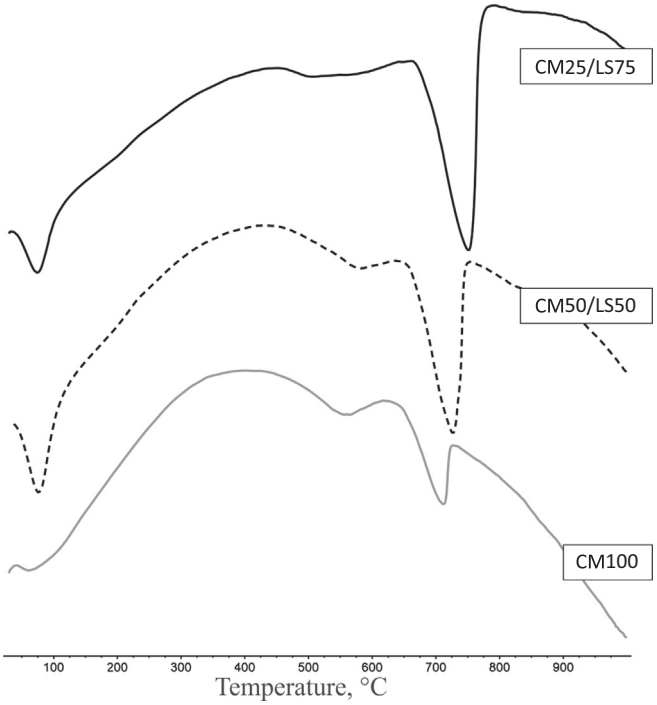

Fig. 9. DSC analysis of hardened pastes.

3.5. The formation of the CM-LS-NSH_5 system

Analysis of the presented experimental procedure allows us to assume the mechanism of formation described below for the CM-LS-NSH_5

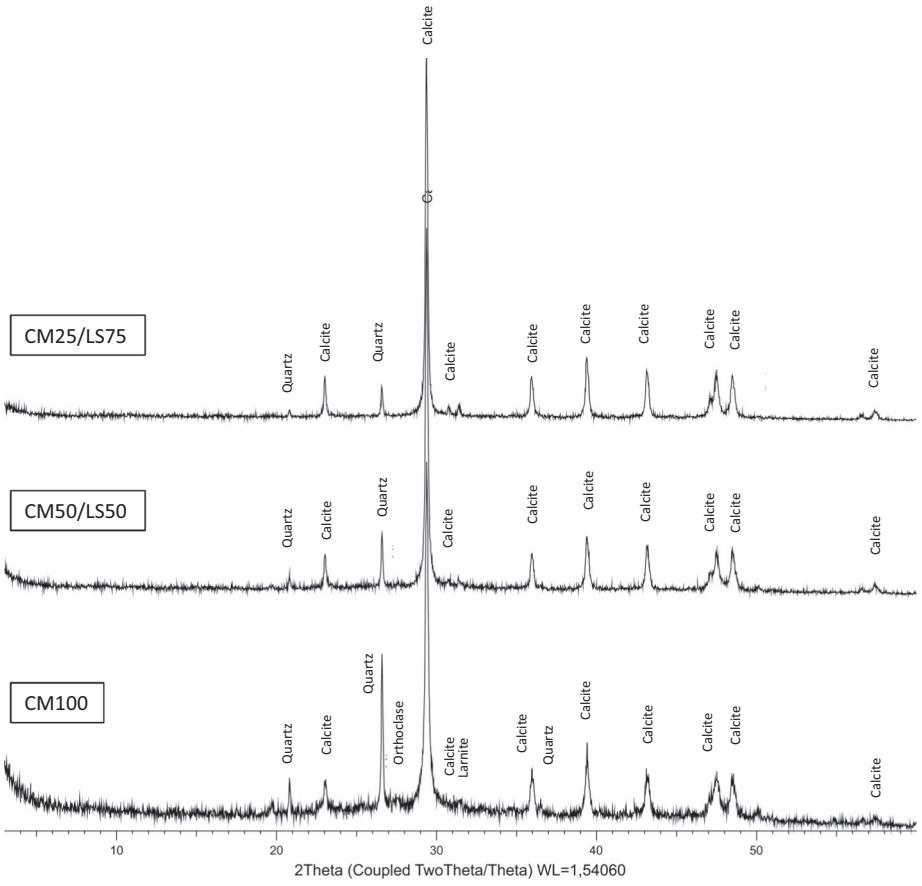

Fig. 8. X-ray diffractograms of the hardened pastes.

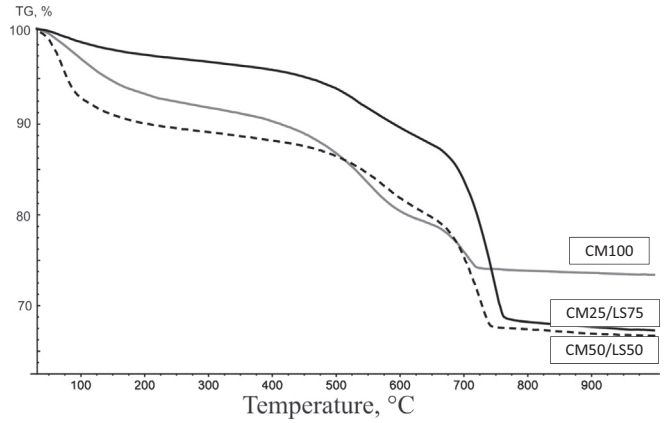

Fig. 10. TG analysis of hardened pastes.

system. The RM is characterized by low content of aluminosilicates (25.77%), which are considered as geopolymer precursors including the most promising constituents – kaolinite (3.45%) and montmorillonite (6.41%). At the same time, many studies have proved that the predominant constituents of marl calcite and quartz demonstrate good compatibility with the geopolymer-based mineral matrix [36,45,61–63]. Thus, RM consists of aluminosilicate constituents which are able to form an alkali aluminosilicate gel after calcination, as well as "inert" calcium carbonate and silica-based constituents which are compatible with that binder gel. However, as has been mentioned in Sec. 2.2, a good strength of the CM-based geopolymer was obtained only after calcination at a temperature of 800 °C. This is because, as the thermal analysis (Fig. 3) of RM showed, the temperatures of kaolinite dehydroxylation are 510 and 760 °C respectively. Moreover, it can be concluded from thermal analysis which demonstrate that the highest mass loss caused by partial calcite decarbonation and kaolinite dehydroxylation and occurs in range 630–780 °C – 19.31% (whereas total mass loss is 26.99%) of raw marl that along with dehydroxylated aluminosilicates the strength formation process of geopolymer is also supported by CaO. We also concluded that the marl of a given chemical-mineralogical composition after calcination at temperatures 600 and 700 °C and through the use of an alkali activator can be considered as a precursor for a geopolymer with a compressive strength lower than 30 MPa. A higher compressive strength may be obtained by using higher calcination temperatures leading to the formation of reactive Ca, which is a key contributor to the formation of hydrous calcium silicates. Many studies mentioned the coexistence of the N-A-S-H and C-A-S-H

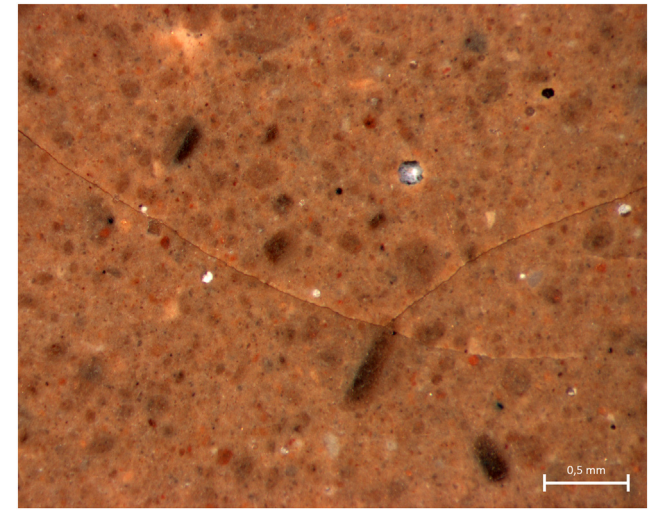

Fig. 12. Optical microscopy of the hardened paste based on CM100.

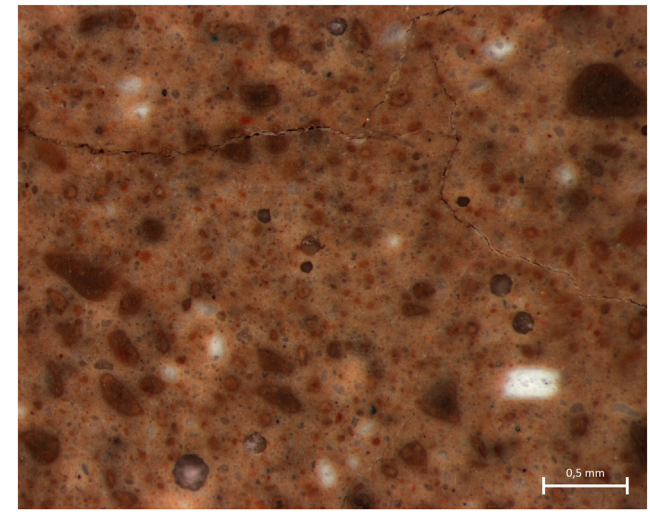

Fig. 13. Optical microscopy of the hardened paste based on CM50/LS50.

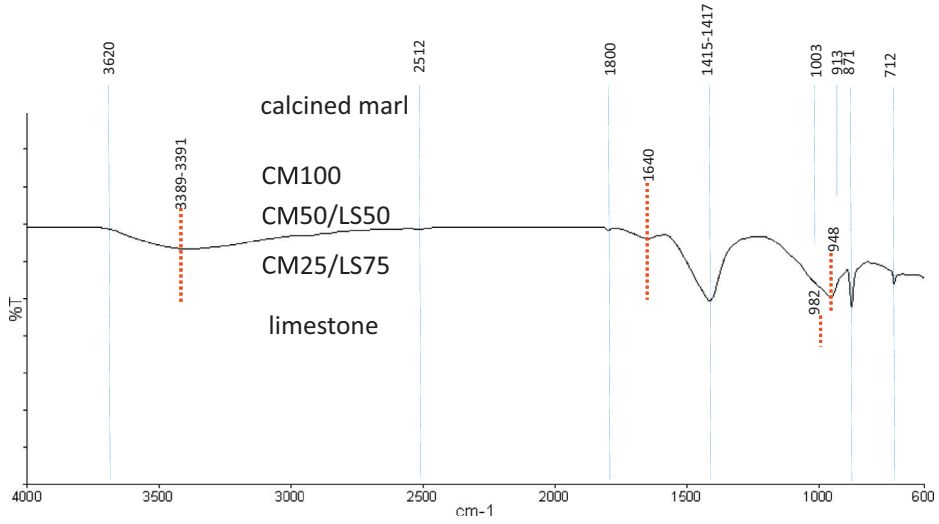

Fig. 11. FTIR analysis of hardened pastes.

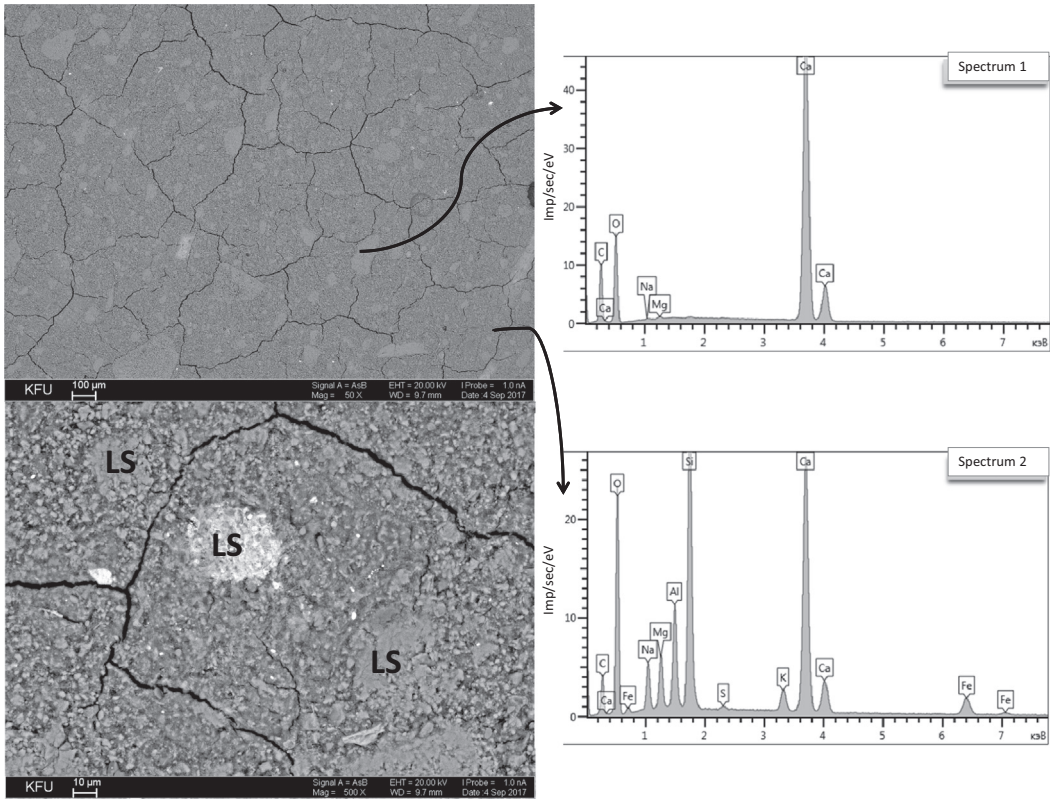

Fig. 14. SEM microscopy of the hardened paste based on CM50/LS50.

binder gels in blended activated systems incorporated with the Ca-source [64–67]. The mechanism of effective coexistence of the different binder gels is explained by the C-A-S-H-gel filling the pores and voids in the geopolymer network like a microaggregate, as well as by the gel bridging the gaps between the different reaction products and unreacted particles [67]. Based on presented data of DSC/TG, FTIR, and microscopy analyses alkali activation of calcined at 800 °C marl containing reactive Ca, Si, Al by NSH_5 with high probability results in formation of mixed N-A-S-H/C-A-S-H gel which binds particles of calcite and quartz. C-A-S-H may be formed not only through the reaction of calcined aluminosilicates with the reactive Ca and NSH_5 but also through the hydration of larnite. Relict calcite appears on the X-ray diffractograms, but calcite may be also newly formed as a result of the carbonization of CaO.

The incorporation of up to 50% calcium carbonate in replacing calcined marl delays the reactions in blended activated systems because of the reduction of the reactive phase. The incorporation of calcium carbonate also improves the compressive strength of the CM-geopolymer, which is consistent with the findings of several studies [36,44,46]. Any further increase in the LS content deteriorates the compressive strength of the hardened pastes. In this study, the specific surface area of the LS was lower (3700 cm^2/g) than that of the CM (5000 cm^2/g). This suggests that there is potential for further strength improvement by increasing the fineness of the LS [6,40]. The reasons for the compatibility between the CM-based matrix and the LS powder resulting in a high content of mineral addition added in the geopolymer and beneficial effects on the compressive strength of the hardened inorganic matrix are as follows.

- The incorporation of the LS powder increases the amount of binder aluminosilicate gels such that it can (i) slightly dissolve in the liquid phase of the fresh geopolymer paste, (ii) enhance the release of Al and Si ions from the aluminosilicate precursor, (iii) increase the effectiveness of the activator/aluminosilicate ratio, (iv) act as nucleation sites for the reaction products [60,68,69]. The higher amount of binder gels in the CM-based pastes mixed with 50% LS is supported by the DSC/TG analyses (Fig. 9), which demonstrated that the sample with 50% LS powder (CM50/LS50) has the highest mass loss of 9.19%, caused by the loss of evaporable water from the binder gels compared to the CM100 sample where the mass loss was 5.96%, and the CM25/LS75 sample with a mass loss of 1.89% in the 50–150 °C temperature range.
- The incorporation of LS powder positively affects the porosity of the hardened activated mixed systems, which is one of the contributing factors in the relationship between the macro- and microstructures and the compressive strength of hardened blended systems [6]. This has been confirmed by compressive strength tests.
- The vivid adhesion between the geopolymer matrix and the LS particles is based not only on the alkali-activation but on the chemical-mineralogical affinity of LS and CM [6,40,44]. This is supported by the compressive strength tests and is evident from the optical and SEM microscopy test results (Figs. 12–14).
- Regarding the optimal CM/LS ratio, CM mixed with 50% LS contains sufficient reactive constituents for the formation of sufficient amounts of binding aluminosilicate gels. The increase in the LS content breaks the chemical equilibrium between the reactive Si, Al, Ca and NSH_5; it reduces the amount of gels and the compressive strength of the hardened samples with more than 50% of LS incorporated. This is confirmed by the results of DSC/TG (Figs. 9 and 10) and FTIR (Fig. 11).

4. Conclusion

The objectives of this research were the study of calcined marl with high calcite/aluminosilicates as a precursor for geopolymers, and that of geopolymers incorporated with limestone. It was found that after calcinating marl at 800 °C in order to dehydroxylate the kaolinite and decarbonate the calcite its amorphous phase increases almost twice,

thus making it a good starting material for producing geopolymers with a compressive strength higher than 30 MPa. The alkali activation of marl calcined at 800 °C using hydrous sodium metasilicate (15% by Na_2O) followed by curing at room temperature results in a hardened geopolymer paste with a 28-day compressive strength of 34 MPa. The incorporation of up to 50% limestone, used to replace the calcined marl, into the geopolymer increases the compressive strength of the geopolymer up to 39.2 MPa. The reinforcing mechanism of the blended activated system is based on the (i) chemical-mineralogical affinity and good adhesion between the mineral matrix and limestone, (ii) increase in binder gel amount, and (iii) improvement in the structure of the hardened paste. The main reaction products of the hardened geopolymer and the geopolymer paste incorporated with limestone are N-A-S-H and C-A-S-H, relict marl, and limestone minerals.

These results contribute to the expanding of the raw materials base of geopolymers and the scientific developments of blended activated systems.

References

[1] F. Pacheco-Torgal, J. Labrincha, C. Leonelli, A. Palomo, P. Chindaprasit, Handbook of Alkali-Activated Cements, Mortars and Concretes, Elsevier, 2014.
[2] J.L. Provis, J.S.J. van Deventer, Alkali Activated Materials, State-of-the-Art Report, RILEM, TC 224-AAM, Springer, 2014.
[3] A. Mehta, R. Siddique, An overview of geopolymers derived from industrial by-products, Constr. Build. Mater. 127 (2016) 183–198.
[4] J.L. Provis, S.A. Bernal, Milestones in the analysis of alkali-activated binders, J. Sust. Cem.-Based Mater. (2) (2014) 74–84.
[5] S.A. Bernal, E.D. Rodríguez, A.P. Kirchheim, J.L. Provis, Management and valorization of wastes through use in producing alkali-activated cement materials, J. Chem. Technol. Biotechnol. 91 (9) (2016) 2365–2388.
[6] N.R. Rakhimova, R.Z. Rakhimov, A review on alkali-activated slag cements incorporated with supplementary materials, J. Sust. Cem.-Based Mater. 3 (1) (2014) 61–74.
[7] A.M. Rashad, Alkali-activated metakaolin: a short guide for civil Engineer – an overview, Constr. Build. Mater. 41 (2013) 751–765.
[8] A.M. Rashad, A comprehensive overview about the influence of different admixtures and additives on the properties of alkali-activated fly ash, Mater. Des. 53 (2014) 1005–1025.
[9] Y.C. Diaz, S.S. Berriel, U. Heierli, A.R. Favier, I.R. Sanchez Machado, K.L. Scrivener, J. Fernando, M. Hernandez, G. Habert, Limestone calcined clay cement as a low-carbon solution to meet expanding cement demand in emerging economies, Dev. Eng. 2 (2017) 82–91.
[10] B. Lothenbach, K.L. Scrivener, R.D. Hooton, Supplementary cementitious materials, Cem. Concr. Res. 41 (2011) 1244–1256.
[11] H.M. Ludwig, CO_2-arme Zemente fur nachhaltige Betone, in: H.B. Fischer, C. Boden, M. Neugebauer (Eds.), Proceedings of 19. Internationale Baustofftagung Ibausil, F.A. Finger-Institute, Weimar, Germany, 2015, pp. 7–32.
[12] R.Z. Rakhimov, N.R. Rakhimova, A.R. Gaifullin, V.P. Morozov, Influence of the calcinated light loam on the properties of the hardened Portland cement paste, Rom. J. Mater. 4 (2017) 484–490.
[13] R.Z. Rakhimov, N.R. Rakhimova, A.R. Gaifullin, V.P. Morozov, Properties of Portland cement paste enriched with addition of calcined marl, J. Build. Eng. 11 (2017) 30–36.
[14] I. Aldabsheh, H. Khoury, J. Wastiels, H. Rahier, Dissolution behavior of Jordanian clay-rich materials in alkaline solutions for alkali activation purpose. Part I, Appl. Clay Sci. 115 (2015) 238–247.
[15] S. Boussen, D. Sghaier, F. Chaabani, B. Jamoussi, S.B. Messaoud, A. Bennour, The rheological, mineralogical and chemical characteristic of the original and the Na_2CO_3-activated Tunisian swelling clay (Aleg Formation) and their utilization as drilling mud, Appl. Clay Sci. 118 (2015) 344–353.
[16] J. Dietel, L.N. Warr, M. Bertmer, A. Steudel, G.H. Grathoff, K. Emmerich, The importance of specific surface area in the geopolymerization of heated illitic clay, Appl. Clay Sci. 139 (2017) 99–107.
[17] D.M. González-García, L. Téllez-Jurado, F.J. Jiménez-Álvarez, H. Balmori-Ramírez, Structural study of geopolymers obtained from alkali-activated natural pozzolan feldspars, Ceram. Int. 43 (2017) 2606–2613.
[18] S.S. Nenadovic, L.M. Kljajevic, M.A. Nesic, M.Z. Petkovic, K.V. Trivunac, V.B. Pavlovic, Structure analysis of geopolymers synthesized from clay originated from Serbia, Environ. Earth Sci. 1 (2017) (2017) 76–79.
[19] S. Ng, H. Justnes, Influence of dispersing agents on the rheology and early heat of hydration of blended cements with high loading of calcined marl, Cem. Concr. Compos. 60 (2015) 123–134.
[20] A. Buchwald, M. Hohmann, C. Kaps, The suitability of different clay resources in respect to form geopolymeric binders, Proceedings of International Conference on Alkali Activated Materials: Research, Production and Utilization, Prague, 2007, pp. 137–148.
[21] A. Buchwald, M. Hohmann, K. Posern, E. Brendler, The suitability of thermally activated illite/smectite clay as raw material for geopolymer binders, Appl. Clay Sci. 46 (3) (2009) 300–304.
[22] H. Xu, J.S.J. van Deventer, The geopolymerisation of alumino-silicate minerals, Int. J. Miner. Process. 59 (3) (2000) 247–266.
[23] H. Xu, J.S.J. van Deventer, Factors affecting the geopolymerization of alkali-feldspars, Miner. Metall. Process. 19 (4) (2002) 209–214.
[24] K.J.D. MacKenzie, D.R.M. Brew, R. Fletcher, R. Vagana, Formation of aluminosilicate geopolymers from 1:1 layer-lattice minerals pre-treated by various methods: a comparative study, J. Mater. Sci. 42 (2007) 4667–4674.
[25] S.A. Bernal, J.L. Provis, R. Mejía de Gutierrez, V. Rose, Evolution of binder structure in sodium silicate-activated slag-metakaolin blends, Cem. Concr. Compos. 33 (1) (2011) 46–54.
[26] S.A. Bernal, J.L. Provis, V. Rose, R. Mejía de Gutiérrez, High-resolution x-ray diffraction and fluorescence microscopy characterization of alkali-activated slag-metakaolin binders, J. Am. Ceram. Soc. 96 (6) (2013) 1951–1957.
[27] A. Buchwald, R. Tatarin, D. Stephan, Reaction progress of alkaline-activated metakaolin-ground granulated blast furnace slag blends, J. Mater. Sci. 44 (20) (2009) 5609–5617.
[28] P. Duan, C. Yan, W. Zhou, A novel water permeable geopolymer with high strength and high permeability coefficient derived from fly ash, slag and metakaolin, Adv. Powder Technol. 28 (2017) 1430–1434.
[29] H.M. Khater, M. Ezzat, A.M. El Nagar, Alkali activated eco-friendly metakaolin/slag geopolymer building bricks, Chem. Mater. Res. 8 (1) (2016) 21–32.
[30] I. Perna, T. Hanzlícek, The setting time of a clay-slag geopolymer matrix: the influence of blast-furnace-slag addition and the mixing method, J. Clean. Prod. 112 (2016) 1150–1155.
[31] M. Antoni, J. Rossen, F. Martirena, K. Scrivener, Cement substitution by a combination of metakaolin and limestone, Cem. Concr. Res. 42 (12) (2012) 1579–1589.
[32] A. Arora, G. Sant, N. Neithalath, Ternary blends containing slag and interground/blended limestone: hydration, strength, and pore structure, Constr. Build. Mater. 102 (1) (2016) 113–124.
[33] U. Avila-López, J.M. Almanza-Robles, J.I. Escalante-García, Investigation of novel waste glass and limestone binders using statistical methods, Constr. Build. Mater. 82 (2015) 296–303.
[34] F. Allali, E. Joussein, N. Idrissi Kandri, S. Rossignol, The influence of calcium content on the performance of metakaolin-based geomaterials applied in mortars restoration, Mater. Des. 103 (2016) 1–9.
[35] L. Chong, C. Shi, C.J. Yang, H. Jia, Effect of limestone powder on the water stability magnesium phosphate cement-based materials, Proceedings of the 14th International Congress on the Chemistry of Cement, Beijing, China, 2015, p. 421.
[36] A. Cwirzen, J.L. Provis, V. Penttala, K. Habermehl-Cwirzen, The effect of limestone on sodium hydroxide-activated metakaolin-based geopolymers, Constr. Build. Mater. 66 (2014) 53–62.
[37] X. Gao, Q.L. Yu, H.J.H. Brouwers, Properties of alkali activated slag–fly ash blends with limestone addition, Cem. Concr. Compos. 59 (2015) 119–128.
[38] P. Hawkins, P. Tennis, R. Detwiler, The Use of Limestone in Portland Cement: A State-of-the-art Review, Portland Cement Association, Illinois, 2003.
[39] A.J. Moseson, D.E. Moseson, M.W. Barsoum, High volume limestone alkali-activated cement developed by design of experiment, Cem. Concr. Compos. 34 (3) (2012) 328–336.
[40] N.R. Rakhimova, R.Z. Rakhimov, N.I. Naumkina, A.F. Khuzin, Y.N. Osin, Influence of limestone content, fineness, and composition on the properties and microstructure of alkali-activated slag cement, Cem. Concr. Compos. 72 (2016) 268–274.
[41] M.X. Peng, Z.H. Wang, Q.G. Xiao, F. Song, W. Xie, L.C. Yu, H.W. Huang, S.J. Yi, Effects of alkali on one-part alkali-activated cement synthesized by calcining bentonite with dolomite and Na_2CO_3, Appl. Clay Sci. 139 (2017) 64–71.
[42] A.R. Sakulich, E. Anderson, C. Schauer, M.W. Barsoum, Mechanical and microstructural characterization of an alkali-activated slag/limestone fine aggregate concrete, Constr. Build. Mater. 23 (2009) 2951–2959.
[43] A. Vimmrova, M. Keppert, O. Michalko, R. Cerny, Calcined gypsum–lime–metakaolin binders: design of optimal composition, Cem. Concr. Compos. 52 (2014) 91–96.
[44] C.K. Yip, J.L. Provis, G.C. Lukey, J.S.J. Deventer, Carbonate mineral addition to metakaolin-based geopolymers, Cem. Concr. Compos. 30 (3) (2008) 979–985.
[45] A. Aboulayt, M. Riahi, T.M. Ouazzani, H. Hannache, M. Gomina, R. Moussa, Properties of metakaolin based geopolymer incorporating calcium carbonate, Adv. Powder Technol. 28 (2017) 2393–2401.
[46] J. Qian, M. Song, Study on influence of limestone powder on the fresh and hardened properties of early age metakaolin based geopolymer, Proceedings of 1st International Conference on Calcined Clays for Sustainable Concrete, Lausanne, 2015, pp. 235–259.
[47] E.E. Avarez-Ayuso, X. Querol, F. Plana, A. Alastuey, N. Moreno, M. Izquierdo, O. Font, T. Moreno, S. Diez, E. Vazquez, M. Barra, Environmental, physical and structural characterisation of geopolymer matrixes synthesised from coal combustion fly ashes, J. Hazard. Mater. 154 (2008) 175–183.
[48] V.F.F. Barbosa, K.J.D. MacKenzie, C. Thaumaturgo, Synthesis and characterisation of materials based on inorganic polymers of alumina and silica: sodium polysialate polymers, Int. J. Inorg. Mater. 2 (2000) 309–317.
[49] H. Boke, O. Cizer, B. Ipekoglu, E. Ugurlu, K. Serifaki, G. Toprak, Characteristics of lime produced from limestone containing diatoms, Constr. Build. Mater. 22 (2008) 866–874.
[50] A. Sdiri, T. Higashi, T. Hatta, F. Jamoussi, N. Tase, Mineralogical and spectroscopic characterization, and potential environmental use of limestone from the Abiod formation, Tunisia, Environ. Earth Sci. 61 (6) (2010) 1275–1287.
[51] L.N. Tchadjié, J.N.Y. Djobo, N. Ranjbar, H.K. Tchakouté, B.B.D. Kenne, A. Elimbi, D. Njopwouo, Potential of using granite waste as raw material for geopolymer synthesis, Ceram. Int. 42 (2015) 3046–3055.
[52] a J.D. Russel, Infrared Spectroscopy of Inorganic Compounds, Laboratory Mehods

in Infrared Spectroscopy, Wiley, New York, 1987;
b B. Tyagi, C.D. Chudasama, R.V. Jasra, Determination of structural modification in acid activated montmorillonite clay by FT-IR spectroscopy, Spectrochim. Acta A 64A (2006) 273–278.
[53] a H. Van Der Marel, Atlas of Infrared Spectroscopy of Clay Minerals and Their Admixtures, Elsevier, Amsterdam, 1976;
b K. El Hafid, M. Hajjaji, Alkali-etched heated clay: microstructure and physical/mechanical properties, J. Asian Ceramic Soc. 4 (2016) 234–242.
[54] H. Rahier, J.F. Denayer, B. Van Mele, Low-temperature synthesized aluminosilicate glasses. Part IV. Modulated DSC study on the effect of particle size of metakaolinite on the production of inorganic polymer glasses, J. Mater. Sci. 38 (2003) 3131–3136.
[55] H. Rahier, W. Simons, B. Van Melle, M. Biesemans, Low temperature synthesized aluminosilicate glasses Part III. Influence of composition of the silica solution on production, structure and properties, J. Mater. Sci. 32 (1997) 2237–2247.
[56] T. Bakharev, Resistance of geopolymer materials to acid attack, Cem. Concr. Res. 35 (2005) 658–670.
[57] I. Garcia-Lodeiro, A. Palomo, A. Fernández-Jiménez, D.E. Macphee, Compatibility studies between N-A-S-H and C-A-S-H gels. Study in the ternary diagram Na_2O–CaO–Al_2O_3–SiO_2–H_2O, Cem. Concr. Res. 41 (2011) 923–931.
[58] P. Saravanapavan, L. Hench, Mesoporous calcium silicate glasses I. Synthesis, J. Non-Cryst. Solids 318 (2003) 1–13.
[59] V. Stubican, R. Roy, Infrared spectar of layer structure silicate, J. Am. Ceram. Soc. 44 (1961) 625–627.
[60] N.R. Rakhimova, Properties and microstructural characteristics of alkali-activated slag-blended cements, Rom. J. Mater. 45 (2) (2015) 105–116.
[61] A.M. Rashad, A.A. Hassan, S.R. Zeedan, An investigation on alkali-activated Egyptian metakaolin pastes blended with quartz powder subjected to elevated temperatures, Appl. Clay Sci. 132–133 (2016) 366–376.
[62] H.K. Tchakoute, C.H. Rüscher, J.N.Y. Djobo, B.B.D. Kenne, D. Njopwouo, Influence of gibbsite and quartz in kaolin on the properties of metakaolin-based geopolymer cements, Appl. Clay Sci. 107 (2015) 188–194.
[63] Q. Wan, F. Rao, S. Song, D.F. Cholico-Gonzalez, N.L. Ortiz, Combination formation in the reinforcement of metakaolin geopolymers with quartz sand, Cem. Concr. Compos. 80 (2017) 115–122.
[64] S. Alonso, A. Palomo, Alkaline activation of metakaolin and calcium hydroxide mixtures: influence of temperature, activator concentration and solids ratio, Mater. Lett. 47 (2001) 55–62.
[65] S. Boonjaeng, P. Chindaprasirt, K. Pimraksa, Lime-calcined clay materials with alkaline activation: phase development and reaction transition zone, Appl. Clay Sci. 95 (2014) 357–364.
[66] X. Guo, H. Shi, Metakaolin-, fly ash- and calcium hydroxide-based geopolymers: effect of calcium on performance, Adv. Cem. Res. 27 (10) (2015) 559–566.
[67] C.K. Yip, G.C. Lukey, S.Js. Deventer, The coexistence of geopolymeric gel and calcium silicate hydrate gel at the early stage of alkaline activation, Cem. Concr. Res. 35 (9) (2005) 1688–1697.
[68] A. Cwirzen, V. Penttala, RPC mix optimization by determination of the minimum water requirement of binary and polydisperse mixtures, Proceedings of the International Symposium on Innovation and Sustainability of Structures in Civil Engineering, Nanjing, China, 2005.
[69] T. Oey, A. Kumar, J.W. Bullard, N. Neithalath, G. Sant, The filler effect: the influence of filler content and surface area on cementitious reaction rates, J. Am. Ceram. Soc. 96 (2013) 1978–1990.